Broadband Microwave Frequency Characterization of 3-D Printed Materials

Article *in* IEEE Transactions on Components and Packaging Technologies · December 2013

DOI: 10.1109/TCPMT.2013.2273306

3 authors, including:

Raymond Rumpf
University of Texas at El Paso
68 PUBLICATIONS **746** CITATIONS

SEE PROFILE

Broadband Microwave Frequency Characterization of 3-D Printed Materials

Paul I. Deffenbaugh, *Member, IEEE*, Raymond C. Rumpf, *Member, IEEE*, and Kenneth H. Church, *Member, IEEE*

***Abstract*— 3-D printing allows increased design flexibility in the fabrication of microwave circuits and devices and is reaching a level of maturity that allows for functional parts. Little is known about the RF and microwave properties of the standard materials that have been developed for 3-D printing. This paper measures a wide variety of materials over a broad spectrum of frequencies from 1 MHz to 10 GHz using a variety of well-established measurement methods.**

***Index Terms*— 3-D printing, direct-digital manufacturing, microwave materials measurement, printed electronics.**

I. Introduction

STATE of the art 3-D printing is capable of fabricating structurally functional parts. The advantages of 3-D printing include time saving and the ability to create new devices that cannot be made using standard fabrication techniques. Recently, researchers demonstrated the addition of electronics by combining 3-D printing and printed electronics [1]. These electrically functional devices enhance the potential of 3-D structures by offering greater design flexibility and tighter integration of functionality than the current process, where printed circuit boards are placed into injection-molded plastic cases. The majority of 3-D electronic structures demonstrated have been in the dc or low frequency regime [1]. Some larger scale microwave devices have been demonstrated such as copper electroless-plated devices [2]–[4], ceramic SL [5]–[12], and microwave metamaterial structures [13], [14] (this device has since been successfully fabricated and tested). It is clear that almost all high demand electronic devices must have some type of wireless capability, from the five-plus radios in cell phones down to keyless entry for automotive [15] and building access and RFID [16], [17]. Studying RF electronic structures is important but fundamental characterization needs to be done. Microwave frequency characterization of 3-D printable materials is crucial for successful design of microwave circuits that can be fabricated into structures. Loss tangent ($\tan\delta$) allows designers to balance requirements for low-loss performance with requirements for low-cost fabrication and print quality. Dielectric constant is critical because it governs the characteristic impedance of microwave transmission lines in the material that affects reflection loss, it also governs coupling between components in a circuit, and affects the bandwidth of the system. Broadband characterization captures the frequency-dependent nature of these parameters and allows this data to be used in designs at any frequency rather than just a single band of frequencies. Broadband material characterization is important for high-speed digital signals whose frequency spectra are large and frequency dispersion because of varying dielectric constant that can become an issue. Such data for these materials do not exist and this paper seeks to characterize materials printed using fused deposition modeling (FDM) [18] and stereo lithography (SL) [19] technologies. These two technologies are the most mature for 3-D dielectrics. Future researches will determine which materials are suitable for specific applications; however, preliminary results show that FDM exhibits lower microwave loss but low print resolution and a rough surface finish, whereas SL exhibits excellent resolution and a smooth surface finish but has more loss.

Manuscript received February 28, 2013; revised June 4, 2013; accepted July 5, 2013. Date of publication August 2, 2013; date of current version December 9, 2013. This work was supported in part by the Texas Office of the Governor, Rick Perry, under the Texas Emerging Technologies Fund. Recommended for publication by Associate Editor D. G. Kam upon evaluation of reviewers' comments.

P. I. Deffenbaugh was with the W. M. Keck Center for 3-D, the University of Texas, El Paso, TX 79902 USA (e-mail: pdeffenbaugh@miners.utep.edu).

R. C. Rumpf is with the EMLab, Keck Center, University of Texas, El Paso, TX 79902 USA (e-mail: rcrumpf@utep.edu).

K. H. Church is with the Keck Center, University of Texas, El Paso, TX 79902 USA, and also with nScrypt, Inc., Orlando, FL 32826 USA (e-mail: khchurch@utep.edu).

Color versions of one or more of the figures in this paper are available online at http://ieeexplore.ieee.org.

Digital Object Identifier 10.1109/TCPMT.2013.2273306

II. Overview of Methods

The materials were characterized over several frequency bands using different well-established measurement techniques, the I–V capacitance method, the radio frequency current–voltage (RF-I–V) method, and the Nicholson–Ross–Weir (NRW) method [20], [21]. The methods are listed in Table I, discussed in the following sections, and the results of these measurements are shown in the Appendix in Tables IV–VII.

A. Method 1: LCR Meter, 1 MHz, 2 MHz

An Agilent E4980A precision LCR meter [22] with an Agilent 16451B dielectric test fixture [23] was used to measure materials at 1 and 2 MHz, compliant with ASTM D150 [24]. This instrument works using the material under test as the dielectric in a capacitor and measuring the ac current–voltage (I–V) relationship to determine

TABLE I
MEASUREMENT METHODS

Frequency	Method	Error in ε_r	Error [b] in tanδ
1 MHz, 2 MHz	LCR Meter	≤3.7% [a]	20 – 100% [c]
100 MHz – 1 GHz	Impedance Analyzer	≤21% [a]	25 – 300% [c]
8.2 – 11 GHz	Nicholson-Ross-Weir Waveguide	≤5.8% [b]	10 – 300% [d]

[a]Maximum estimated error.
[b]Maximum standard deviation from sample sets.
[c]Approximate range of estimated errors.
[d]Approximate range of standard deviations from samples sets.

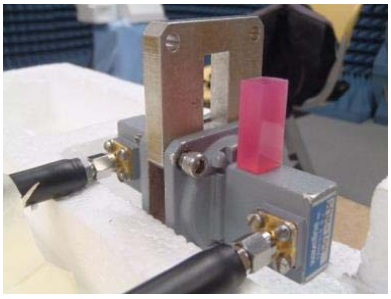

Fig. 1. X-band waveguide measurement setup.

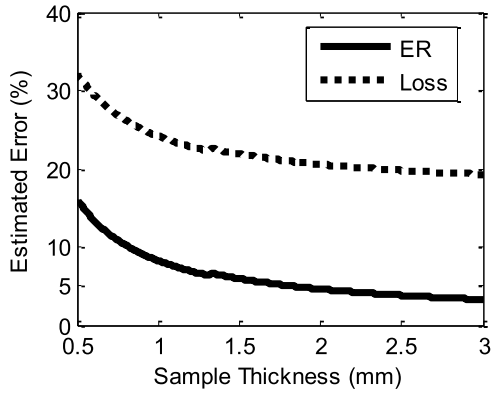

Fig. 2. Estimated error in LCR meter measurement versus sample thickness. Solid line: estimated error in dielectric constant, ε_r. Dashed line: estimated error in loss tangent. Condition: $\varepsilon_r = 3.5$, $\tan\delta = 0.035$, $f = 2$ MHz, $d = 38$ mm, and Vs $= 1$ V.

the complex impedance that is converted to dielectric constant and loss tangent, using physical dimensions and basic equations.

Impedances on the order of 50 Ω–50 kΩ are preferred for accuracy [23] page B-1. Assuming dielectric constants on the order of 1.9–3.5, a sample thickness of 3 mm is selected so that the measured impedances range from 6.8 Ω to 25 kΩ from 1–2 MHz, thus falling within the preferred accuracy range. Estimated error equations are given in Agilent equipment documentation [23] and shown against material thickness in Fig. 2. Although the sample holder allows for samples up to 10 mm in thickness and error seems to reduce with increasing sample thickness, a thickness of 3 mm was selected so as to balance the error of the impedance analyzer that shows increased error with increasing sample thickness. Choosing a single sample thickness allows only one set of samples to be fabricated.

B. Method 2: Impedance Analyzer, 100 MHz–1 GHz

An Agilent E4991A-002 impedance analyzer [25], [26] with Agilent 16453A dielectric test fixture was used to measure materials from 100 MHz to 1 GHz. This instrument works on a similar principle to the LCR meter. The computation of capacitance and loss tangent from the measured impedance is, however, performed by software internal to the unit, which considers the fixture geometry automatically. Unlike the LCR meter, which uses a simple low-frequency I–V measurement technique, impedance measurement is performed using a RF-I–V method [21, pp. 2–16], [27].

C. Method 3: X-Band Waveguide and 8.2–12.4 GHz

Material samples were fabricated to fit WR-90 waveguide designed for 8.2–12.4 GHz (see Fig. 1). Through-reflect-line calibration was performed at the waveguide ports using a shorting plate and the 1/4-wave (7.63-mm length) sample holder waveguide section. S-parameter data was taken using an Agilent N5245A PNA-X vector network analyzer, and the NRW method [28]–[30] was applied to extract the dielectric constant and loss tangent.

Samples tended to have an approximate dielectric constant of 3.0. These materials were fabricated to 7.63-mm thick to match a readily available 1/4-wavelength waveguide section. This results in an electrical length of ∼1/2 wavelength in the frequency range from 11 to 12.4 GHz. It is known that when the sample thickness is close to 1/2 wavelength, the measured S-parameter data exhibits a singularity (near 100% transmission and 0% reflection) and the material parameters exhibit magnified errors [31], [32]. To mitigate this effect, data in the range 11–12.4 GHz is omitted.

III. FABRICATION

The W. M. Keck Center for 3-D Innovation (the Keck Center) at the University of Texas at El Paso offers a broad selection of additive manufacturing technologies and materials. Materials and technologies were selected for measurement based on availability and estimated suitability for microwave device fabrication.

FDM parts were fabricated using a Stratasys FDM Titan and a T16 tip (406 μm) and 254-μm layer thickness. Three of the most common FDM-printable materials were printed in the Keck Center:

1) polycarbonate (PC) from Stratasys;
2) acrylonitrile butadiene styrene (ABS) as Stratasys ABS-M30;
3) Stratasys PC-ABS blend.

SL parts were fabricated using a 3-D Systems Viper si2, operated in high resolution mode, producing a layer thickness of 50.8 μm using a laser beam diameter of 76.2 μm. Several materials were printed at the Keck Center:

1) Prototherm UV-cured;
2) Prototherm thermally cured;
3) DSM Somos White;
4) Watershed 11122.

Additional SL materials were provided courtesy of DSM Somos:

1) 9120;
2) 9420;
3) DMX-SL 100;
4) NanoForm 15120 UV-cured;
5) NanoTool UV-cured;
6) NeXT;
7) Prototherm UV-cured;
8) Watershed 11122.

For capacitor-plate measurement, samples were fabricated as 50-mm × 50-mm × 3-mm plates. Light sanding and razor blade scraping was performed to remove only the largest FDM surface aberrations and SL support marks. For X-band waveguide measurement, samples were fabricated slightly oversized and computer numeric control machined to 7.63-mm × 10.06-mm × 22.60-mm chunks. Each chunk was machined and sanded to fit as precisely as possible in the X-band waveguide sample holder to minimize air gaps near the waveguide walls.

IV. Measurement and Error

Measuring dielectric constant can be prone to error. Many factors such as dimensional inaccuracies, air gaps, humidity, and calibration affect the measurement. Special care was taken to minimize as many of these effects as possible. Error analyses were carried out when possible to estimate the error present as well as to choose ideal sample dimensions that would minimize the total error. It should be noted that large standard deviations on the order of 100% exist in the measurement of the loss tangent; however, this is predicted by estimated errors of approximately the same magnitude. This is due to the high sensitivity in measuring low loss materials.

A. LCR Meter, 1 MHz, and 2 MHz

Estimated error equations are given for the Agilent E4980A Precision LCR Meter and Agilent 16451B Dielectric Test Fixture [22]. A few interesting results of these estimated error equations are presented in plot form here. Note that these plots have no relation to the measured data but illustrate the behavior of the estimated error using approximate values. Actual estimated error values for the measured data are provided in Tables V and VII.

As shown in Fig. 2, thicker samples ($t = 3$ mm) allow for more accurate measurements. As shown in Fig. 3, minimal variation in accuracy is expected in the measurement range at 1 and 2 MHz. As shown in Fig. 4, in the range of loss tangent values from 0.01 to 0.04 the estimated error will be approximately 20% to 40%. The test signal voltage was chosen to be 1 V as per Fig. 5.

B. Air Gap in Use of LCR Meter, 1 MHz, and 2 MHz

The given equations from the Agilent equipment documentation include inaccuracies internal to the equipment, because of the cable length and sample holder geometry. There is an additional source of error, the uneven air gap between the sample and electrode. Samples cannot be manufactured with perfectly parallel faces resulting in a reduction in overall capacitance. To characterize this source of error, the following model is used. The sample is assumed to have nonparallel

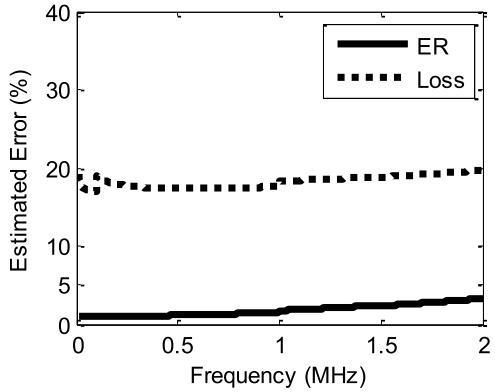

Fig. 3. Estimated error in LCR meter measurement versus frequency. Solid line: estimated error in dielectric constant, ε_r. Dashed line: estimated error in loss tangent. Condition: $\varepsilon_r = 3.5$, $\tan\delta = 0.035$, $d = 38$ mm, $t = 3$ mm, and $V\text{s} = 1$ V.

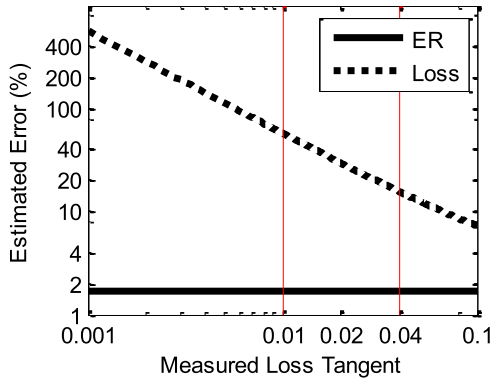

Fig. 4. Estimated error in LCR meter measurement versus loss tangent. Solid line: estimated error in dielectric constant, ε_r. Dashed line: estimated error in loss tangent. Red lines: approximate measurement range. Condition: $\varepsilon_r = 3.5$, $f = 1$ MHz, $d = 38$ mm, $t = 3$ mm, and $V\text{s} = 1$ V.

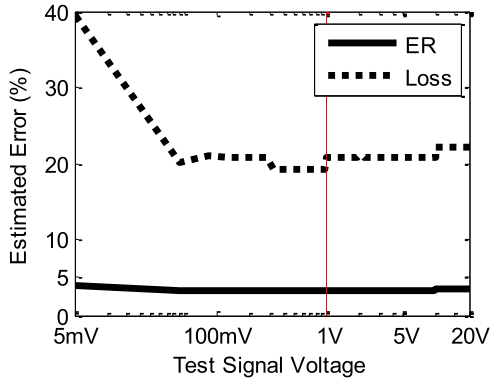

Fig. 5. Estimated error in LCR meter measurement versus test signal voltage. Solid line: estimated error in dielectric constant, ε_r. Dashed line: estimated error in loss tangent. Condition: $\varepsilon_r = 3.5$, $\tan\delta = 0.035$, $f = 2$ MHz, $d = 38$ mm, and $t = 3$ mm.

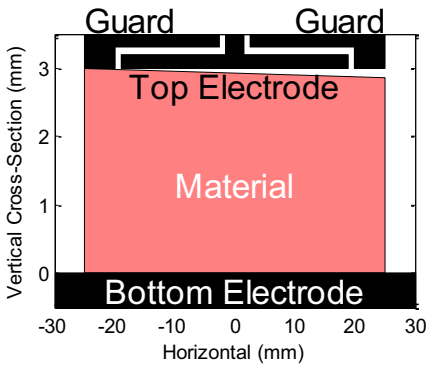

Fig. 6. Diagram of air gap model for an uneven material sample.

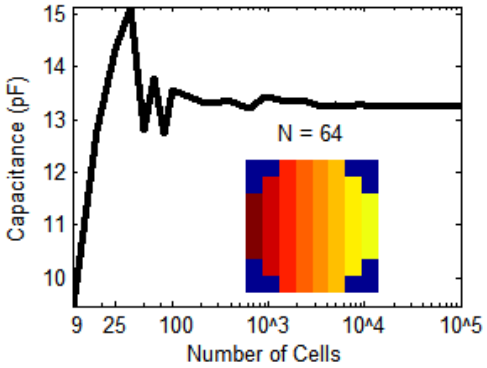

Fig. 7. Convergence of number of cells. Condition: $\varepsilon_r = 3.5$, $t = 3$ mm, $D = 38$ mm, and $g_{\max} = 0.15$ mm. Inset: sample model when $N = 64$.

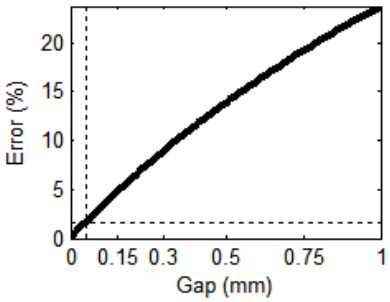

Fig. 8. Estimated error in LCR meter measurement because of air gap. Marker indicates 0.15 mm air gap. Condition: $\varepsilon_r = 3.5$, $t = 3$ mm, and $D = 38$ mm.

faces and the thickness is assumed to be thicker at one side than at the other as shown in Fig. 6. The effects of the fringe guard are removed via open/short compensation on the LCR meter and need not be considered.

A numerical summation is used to compute the actual capacitance of the uneven capacitor. The capacitor area is broken into N_x by N_y small squares and the capacitance of each square C_{sq} is summed to compute the total capacitance. The proper number of squares is determined by checking for convergence as shown in Fig. 7. $N = 10000$ was used. The capacitance contribution of each square is defined as in (1)

$$C_{\text{sq}} = \begin{cases} \frac{\varepsilon_r \varepsilon_0 A}{t + \varepsilon_r g}, & r < D/2 \\ 0, & r \geq D/2. \end{cases} \tag{1}$$

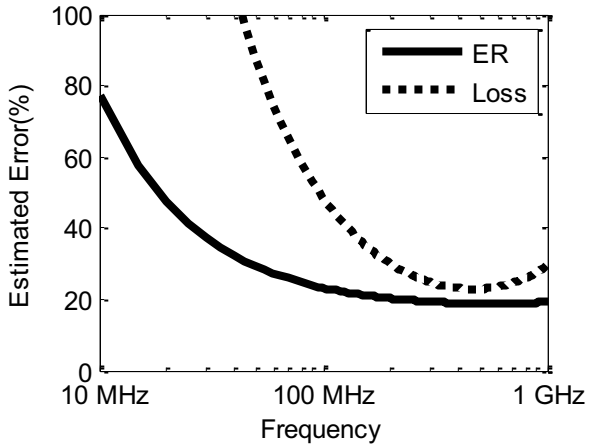

Fig. 9. Estimated error in impedance analyzer measurement versus frequency. Solid line: estimated error in dielectric constant, ε_r. Dashed line: estimated error in loss tangent. Condition: $\varepsilon_r = 2.5$, tanδ = (arbitrary), and $t = 3$ mm.

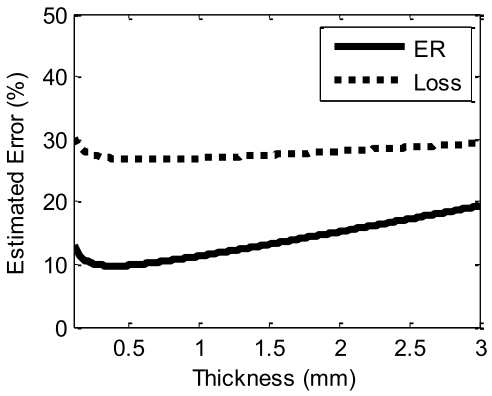

Fig. 10. Estimated error in LCR meter measurement versus sample thickness. Solid line: estimated error in dielectric constant, ε_r. Dashed line: estimated error in loss tangent. Condition: $\varepsilon_r = 2.5$, tanδ = (arbitrary), and $f = 1$ GHz.

The area of each cell A is defined as in (2)

$$A = \frac{D}{N_x}\frac{D}{N_y}. \tag{2}$$

The air gap at each cell $g(x, y)$ and material thickness $t(x, y)$ are defined as in (3) and (4) where TT is the maximum measured sample thickness and $g_{\max}$ is the maximum gap

$$g(x, y) = \frac{x + \frac{D}{2}}{D} g_{\max} \tag{3}$$

$$t(x, y) = T - g(x, y). \tag{4}$$

As shown in Fig. 8, the maximum air gap of the samples fabricated is ~50 μm that adds ~1.68% additional error as compared against a sample without the air gap.

C. Impedance Analyzer and 1 MHz–1 GHz

Estimated error equations are given in the Agilent equipment documentation for the Aglient E4991A RF Impedance-Material Analyzer and Agilent 16453A Dielectric Test

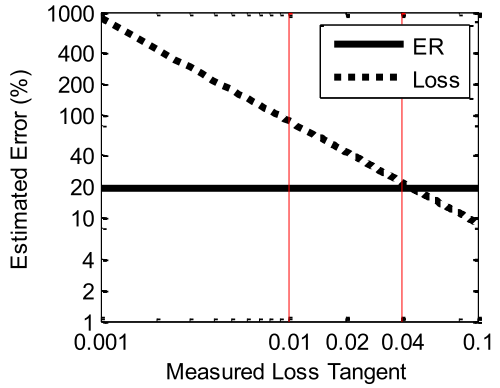

Fig. 11. Estimated error in LCR meter measurement versus loss tangent. Solid line: estimated error in dielectric constant, ε_r. Dashed line: estimated error in loss tangent. Thin vertical lines indicate range where actual materials fell. Condition: $\varepsilon_r = 2.5$, $f = 1$ GHz, and $t = 3$ mm.

TABLE II
LOW-LOSS 3-D PRINTED MATERIALS

Material	Average Loss Tangent
Raw PTFE	0.0016
PC-ABS (FDM)	0.0055
Polycarbonate (FDM)	0.0066
ABS-M30 (FDM)	0.0098
NanoTool (SL)	0.0114
DMX-SL 100 (SL)	0.0130
Prototherm 12120 thermal-cured (SL)	0.0170
"Datasheet" FR-4	0.0180
NanoForm (SL)	0.0240
Prototherm 12120 UV-cured (SL)	0.0368

Note: The data given here are averages across frequency and should not be used because the frequency-dependent nature of these quantities is effectively masked. These values are given for qualitative material-to-material comparison only.

Fixture [25] and are rewritten in (5) and (6)

$$\mathrm{err}_{\varepsilon_r}(\%) = 5 + \left(10 + \frac{0.1}{f}\right)\frac{t}{\varepsilon_r} + 0.25\frac{\varepsilon_r}{t} + \frac{100}{\left|1 - \left(\frac{13}{f\sqrt{\varepsilon_r}}\right)^2\right|} \quad (5)$$

$$\mathrm{err}_{\tan d}(\%) = 0.002 + \frac{0.001}{f}\frac{t}{\varepsilon_r} + 0.004 f + \frac{0.1}{\left|1 - \left(\frac{13}{f\sqrt{\varepsilon_r}}\right)^2\right|}. \quad (6)$$

Of particular note in Fig. 9 is that the error in ε_r is 80% for frequencies ~10 MHz and is < 20% in the range from 100 MHz to 1 GHz. In addition, the error in the loss tangent is so large that the values would be unusable. Thus, only the values from 100 MHz to 1 GHz will be considered. The LCR meter separately provides more accurate data points at 1 and 2 MHz. From Fig. 10, the error in ε_r could be approximately half if the sample thicknesses of 0.4 mm versus 3 mm are used. Fig. 11 shows that in the range of values of loss tangent, errors from 20% to 100% are to be expected.

TABLE III
HIGH DIELECTRIC CONSTANT 3-D PRINTED MATERIALS

Material	Average Dielectric Constant
NanoTool (SL)	3.45
NanoForm 15120 (SL)	3.39
9120 (SL)	3.33
Prototherm 12120 UV-cured (SL)	3.29
9420 (SL)	3.28

Note: The data given here are averages across frequency and should not be used because the frequency-dependent nature of these quantities is effectively masked. These values are given for qualitative material-to-material comparison only.

D. X-Band Waveguide and 8.2–12.4 GHz

A good error analysis of the NRW method is mentioned by Baker–Jarvis [32]; however a simple implementation of this analysis is not available and was not implemented here. Standard deviations of the sample sets are listed in Tables V and VII for frequencies 8.2–11 GHz.

V. CONCLUSION

An important consideration when choosing a material for RF and microwave circuits is the amount of loss that the material introduces. A selection of the 3-D printed materials that were measured in this paper is shown in Table II. Materials printed using thermoplastics and FDM technologies are invariably lower loss than photopolymer-based SL-printed materials. SL offers much higher precision and smoother surface finish than FDM that is important in fabricating microwave devices. There are, however, a few SL materials that show comparable loss to industry-standard FR-4 printed circuit board material. Thus, SL may offer an exciting alternative to FR-4 when the flexibility of 3-D devices (versus the planar nature of FR-4) is considered. The FDM does offer lower loss in applications that are less concerned about resolution and smooth surface finish.

Certain applications demand high dielectric constant to achieve miniaturization in wavelength-dependent structures. For these applications, SL materials may be the better option as shown in Table III. NanoTool and NanoForm incorporate nanoparticles of ceramic that are known to have a high dielectric constant and low loss. New materials are being developed by adding higher concentrations or different types of ceramic [12] to the material to raise the final dielectric constant while at the same time substituting lossy photopolymer for ceramic nanoparticles. The concept of printed and sintered ceramic has been shown to be viable [5]–[12].

Finally, based on the measurements that were performed, 3-D printed materials could be viable options in future RF and microwave devices. In particular, if the dimensional properties of FDM can be tolerated or mitigated, it offers great promise. Otherwise, materials such as NanoTool actually offer lower loss than industry-standard FR-4.

APPENDIX

TABLE IV
DIELECTRIC CONSTANT

Manuf-acturer	Material	Data Sheet	1 MHz	2 MHz	100 MHz	500 MHz	1 GHz	8.2 GHz	9 GHz	10 GHz	11 GHz
Somos	9120		3.83	3.94	3.85	3.58	3.45	2.86	2.83	2.82	2.83
Somos	9420	3.94	3.83	3.97	3.84	3.56	3.44	2.8	2.78	2.68	2.63
Keck FDM	ABS-M30 Lay	2.8	2.63	2.59	2.81	2.79	2.77	2.53	2.54	2.56	2.6
Keck FDM	ABS-M30 St	2.8	NA	NA	NA	NA	NA	2.53	2.56	2.54	2.55
Pure	ABS	2.8	2.79	2.76	2.83	2.81	2.8	2.6	2.62	2.54	2.54
Keck SL	DMX-SL 100	3.7	NA	NA	NA	NA	NA	2.97	2.94	2.98	3.09
Somos	NeXT	3.62	3.65	3.72	3.57	3.38	3.29	2.76	2.8	2.67	2.65
Keck FDM	PC Lay	2.9	2.74	2.7	2.92	2.89	2.86	2.56	2.54	2.57	2.59
Keck FDM	PC St	2.9	NA	NA	NA	NA	NA	2.51	2.5	2.51	2.47
Pure	PC	2.9	2.91	2.87	2.93	2.9	2.89	2.67	2.7	2.59	2.61
Keck FDM	PC-ABS	2.8	2.74	2.7	2.82	2.8	2.77	NA	NA	NA	NA
Keck SL	Prototherm 12120 Th	3.53	3.44	3.38	3.49	3.35	3.28	NA	NA	NA	NA
Keck SL	Prototherm 12120 UV	3.81	3.8	3.78	3.82	3.6	3.49	2.8	2.76	2.75	2.77
Somos	Prototherm 12120 Th	3.53	3.45	3.48	3.3	3.19	3.13	2.84	2.83	2.74	2.71
Somos	Prototherm 12120 UV	3.81	3.68	3.6	3.6	3.42	3.33	2.94	2.96	2.88	2.93
Pure	PTFE	2.1	2.12	2.1	2.07	2.08	2.07	1.96	1.98	1.95	1.97
Keck FDM	NanoForm 15120	3.73	NA	NA	NA	NA	NA	3.17	3.14	3.07	2.97
Somos	NanoForm 15120	3.73	3.75	3.84	3.81	3.66	3.58	3.05	3.05	2.93	2.88
Somos	NanoTool	3.6	3.57	3.52	3.7	3.61	3.56	3.28	3.33	3.2	3.29
Somos	Watershed 11122	3.45	3.44	3.49	3.35	3.19	3.11	2.68	2.71	2.62	2.62
Keck SL	Watershed 11122	3.45	3.57	3.57	3.55	3.36	3.27	NA	NA	NA	NA
Keck SL	White 14120	3.5	3.47	3.35	3.46	3.29	3.2	2.77	2.74	2.75	2.78

Entries marked "NA" indicate that samples of this type were not fabricated.
"Th" = Thermally post-cured, "UV" = UV post-cured only, "Lay" = laying down orientation, "St" = standing up orientation.
Sample dimensions: 1 MHz – 1 GHz: 3 mm thick × 50 mm dia., 8.2-11 GHz: 7.63 mm × 10.06 mm × 22.60 mm

TABLE V
PERCENT STANDARD DEVIATION AND ESTIMATED PERCENTAGE ERROR IN DIELECTRIC CONSTANT

Manuf-acturer	Material	1 MHz	2 MHz	100 MHz	500 MHz	1 GHz	8.2 GHz	9 GHz	10 GHz	11 GHz
Somos	9120	1.9/1.9	2.0/3.7	0.9/17	0.8/15	0.8/17	1.5	1.8	1.9	2.6
Somos	9420	1.4/1.8	0.8/3.7	1.7/17	1.5/15	1.5/17	1.7	1.7	2.3	2.7
KeckFDM	ABS-M30 Lay	0.5/1.3	0.5/2.6	0.8/21	0.7/18	0.7/18	1.1	0.9	1.0	1.4
KeckFDM	ABS-M30 St	NA	NA	NA	NA	NA	1.3	1.6	2.1	2.5
Pure	ABS	0/1.3	0/3.5	0/21	0/17	0/18	0.5	0.8	0.3	0.8
KeckSL	DMX-SL 100	NA	NA	NA	NA	NA	2.1	1.6	2.5	3.1
Somos	NeXT	0.8/1.8	1.0/3.5	0.9/18	0.8/16	0.8/17	0.9	0.9	0.9	1.3
KeckFDM	PC Lay	3.1/1.3	2.1/2.6	2.9/21	3.0/17	2.9/18	2.1	2.0	1.8	1.3
KeckFDM	PC St	NA	NA	NA	NA	NA	0.8	1.4	1.1	1.0
Pure	PC	0/1.4	0/2.7	0/21	0/17	0/18	0.5	0.3	0.8	0.5
KeckFDM	PC-ABS	3.1/1.3	2.1/2.6	0.8/21	0.9/18	0.9/18	NA	NA	NA	NA
Keck SL	Prototherm Th	0.9/1.7	1.2/3.2	0.6/18	0.5/16	0.5/17	NA	NA	NA	NA
Keck SL	Prototherm UV	2.9/1.8	1.4/3.5	1.1/17	1.0/15	1.0/16	2.3	2.5	2.4	3.3
Somos	Prototherm Th	0.4/1.6	1.7/3.2	0.6/19	0.2/16	0.5/17	1.2	1.8	2.8	4.2
Somos	Prototherm UV	0.9/1.8	0.7/3.4	0.8/18	0.8/15	0.7/17	0.8	0.9	1.0	1.9
Pure	PTFE	0/1.0	0/2.2	0/26	2.0/21	0/21	0	0	0	0
KeckFDM	NanoForm 15120	NA	NA	NA	NA	NA	1.5	1.1	3.9	5.8
Somos	NanoForm 15120	0.9/1.8	1.4/3.5	2.6/17	2.5/15	2.4/16	1.8	1.9	2.1	3.1
Somos	NanoTool	1.0/1.6	0.9/3.1	1.7/18	1.6/15	1.6/16	0.6	0.8	0.5	1.7
Somos	Watershed 11122	0.3/1.6	0.6/3.2	1.1/19	0.9/16	1.0/17	2.2	2.1	2.3	2.2
Keck SL	Watershed 11122	0.9/1.8	1.3/3.4	0.6/18	0.5/16	0.5/17	NA	NA	NA	NA
Keck SL	White 14120	1.3/1.7	1.6/3.2	1.1/18	0.9/16	1.0/17	2.2	1.7	3.2	3.0

Entries marked "NA" indicate that samples of this type were not fabricated.
"Th" = Thermally post-cured, "UV" = UV post-cured only, "Lay" = laying down orientation, "St" = standing up orientation.
Notation is "%std. dev. / %est. err". Estimated error is not available for X-band measurements.
Sample dimensions: 1 MHz – 1 GHz: 3 mm thick × 50 mm dia., 8.2-11 GHz: 7.63 mm × 10.06 mm × 22.60 mm

TABLE VI

LOSS TANGENT

Manuf-acturer	Material	1 MHz	2 MHz	100 MHz	500 MHz	1 GHz	8.2 GHz	9 GHz	10 GHz	11 GHz
Somos	9120	0.0196	0.0226	0.0413	0.0426	0.0402	0.0313	0.0348	0.0379	0.0347
Somos	9420	0.0201	0.0234	0.0410	0.0428	0.0406	0.0288	0.0312	0.0384	0.0319
KeckFDM	ABS-M30Lay	0.0069	0.0053	0.0037	0.0033	0.0033	0.0108	0.0138	0.0181	0.0098
KeckFDM	ABS-M30St	NA	NA	NA	NA	NA	0.0075	0.0090	0.0207	0.0130
Pure	ABS	0.0067	0.0049	0.0044	0.0038	0.0031	0.0169	0.0114	0.0151	0.0106
KeckSL	DMX-SL100	NA	NA	NA	NA	NA	0.0115	0.0135	0.0162	0.0130
Somos	NeXT	0.0311	0.0357	0.0344	0.0302	0.0274	0.0253	0.0288	0.0502	0.0305
KeckFDM	PCLay	0.0076	0.0072	0.0050	0.0044	0.0037	0.0073	0.0096	0.0018	0.0066
KeckFDM	PCSt	NA	NA	NA	NA	NA	0.0036	0.0038	0.0059	0.0050
Pure	PC	0.0075	0.0073	0.0052	0.0050	0.0040	0.0020	0.0024	0.0052	0.0049
KeckFDM	PC-ABS	0.0076	0.0072	0.0049	0.0038	0.0038	NA	NA	NA	0.0055
KeckSL	Prototherm12120Th	0.0224	0.0238	0.0244	0.0219	0.0205	NA	NA	NA	0.0226
KeckSL	Prototherm12120UV	0.0171	0.0193	0.0333	0.0346	0.0333	0.0122	0.0130	0.0115	0.0170
Somos	Prototherm12120Th	0.0224	0.0243	0.0223	0.0191	0.0176	0.0074	0.0102	0.0149	0.0196
Somos	Prototherm12120UV	0.0148	0.0161	0.0285	0.0303	0.0293	0.0513	0.0434	0.0437	0.0368
Pure	PTFE	0	0	0.0008	0.0002	0.0001	0.0027	0.0009	0	0.0016
KeckFDM	NanoForm15120	NA	NA	NA	NA	NA	0.0286	0.0257	0.0256	0.0286
Somos	NanoForm15120	0.0131	0.0148	0.0222	0.0229	0.0225	0.0275	0.0221	0.0245	0.0286
Somos	NanoTool	0.0097	0.0096	0.0130	0.0127	0.0122	0.0329	0.0252	0.0255	0.0176
Somos	Watershed11122	0.0236	0.0263	0.0292	0.0271	0.0253	0.0212	0.0235	0.0424	0.0273
KeckSL	Watershed11122	0.0123	0.0312	0.0341	0.0305	0.0282	NA	NA	NA	0.0254
KeckSL	White14120	0.0296	0.0031	0.0321	0.0291	0.0265	0.0214	0.0266	0.0277	0.0246

Entries marked "NA" indicate that samples of this type were not fabricated.
"Th" = Thermally post-cured, "UV" = UV post-cured only, "Lay" = laying down orientation, "St" = standing up orientation.
Values of "0" indicate that the value was so small that it was measured as a negative number due to normal measurement error.
Sample dimensions: 1 MHz – 1 GHz: 3 mm thick × 50 mm dia., 8.2-11 GHz: 7.63 mm × 10.06 mm × 22.60 mm

TABLE VII

PERCENT STANDARD DEVIATION AND ESTIMATED PERCENTAGE ERROR IN LOSS TANGENT

Manuf-acturer	Material	1 MHz	2 MHz	100 MHz	500 MHz	1 GHz	8.2 GHz	9 GHz	10 GHz	11 GHz
Somos	9120	2.4/31	2.6/29	2.3/25	1.1/15	0.8/23	108	98	73	69
Somos	9420	1.3/30	0.8/28	2.1/25	1.9/15	1.8/22	120	112	118	54
KeckFDM	ABS-M30 Lay	0.5/83	0.8/108	39/442	19/203	3.0/267	74	80	63	96
KeckFDM	ABS-M30 St	NA	NA	NA	NA	NA	63	64	87	71
Pure	ABS	0.0/86	0.0/116	0.0/295	0.0/175	0.0/285	1	4	64	5
KeckSL	DMX-SL 100	NA	NA	NA	NA	NA	106	109	140	353
Somos	NeXT	1.2/20	1.3/19	1.9/32	1.6/21	1.0/33	106	106	105	316
KeckFDM	PC Lay	2.1/76	2.7/80	23/263	9.9/149	3.7/236	90	98	349	209
KeckFDM	PC St	NA	NA	NA	NA	NA	185	241	220	272
Pure	PC	0.0/77	0.0/80	0.0/309	0.0/149	0.0/236	939	352	61	649
KeckFDM	PC-ABS	2.1/76	2.7/80	28/45	14/177	4.8/233	NA	NA	NA	NA
Keck SL	Prototherm Th	1.7/27	1.5/27	2.5/31	1.9/29	1.4/44	NA	NA	NA	NA
Keck SL	Prototherm UV	2.1/35	1.9/33	3.3/52	1.4/18	1.0/27	74	78	126	558
Somos	Prototherm Th	0.9/27	2.2/26	0.7/38	0.9/34	1.9/51	648	332	231	368
Somos	Prototherm UV	0.7/40	0.6/38	1.9/38	1.9/21	1.2/31	15	23	30	18
Pure	PTFE	0.0/HIGH	0.0/ HIGH	0.0/ HIGH	135/ HIGH	0/HIGH	0	0	0	0
KeckFDM	NanoForm 15120	NA	NA	NA	NA	NA	96	87	85	109
Somos	NanoForm 15120	0.9/45	0.9/41	2.8/46	3.2/27	3.1/41	99	100	112	125
Somos	NanoTool	0.9/60	1.0/62	4.6/81	3.2/49	2.5/74	28	60	87	71
Somos	Watershed 11122	0.8/25	0.5/25	2.9/39	1.6/24	1.4/35	79	73	62	269
Keck SL	Watershed 11122	5.3/47	2.7/21	4.3/32	1.5/21	1.8/32	NA	NA	NA	NA
Keck SL	White 14120	1.6/21	2.0/185	3.0/35	2.5/22	1.1/34	105	99	97	139

Entries marked "NA" indicate that samples of this type were not fabricated.
"Th" = Thermally post-cured, "UV" = UV post-cured only, "Lay" = laying down orientation, "St" = standing up orientation.
Notation is "std. dev. / est. err". Estimated error is not available for X-band measurements.
Sample dimensions: 1 MHz – 1 GHz: 3 mm thick × 50 mm dia., 8.2-11 GHz: 7.63 mm × 10.06 mm × 22.60 mm

REFERENCES

[1] C. D. Gutierrez, "Three-dimensional structural electronic integration for small satellite fabrication," M.S. thesis, Dept. Electr. Eng., Univ. Texas, El Paso, TX, USA, 2012.

[2] B. Liu, G. Xun, and W. J. Chappell, "Layer-by-layer polymer stereolithography fabrication for three-dimensional RF components," in *IEEE MTT-S Int. Microw. Symp. Dig.*, vol. 2. Jun. 2004, pp. 481–484.

[3] B. Liu, G. Xun, and W. J. Chappell, "Applications of layer-by-layer polymer stereolithography for three-dimensional high-frequency components," *IEEE Trans. Microw. Theory Tech.*, vol. 52, no. 11, pp. 2567–2575, Nov. 2004.

[4] Y. Huang, G. Xun, S. Hajela, and W. J. Chappell, "Layer-by-layer stereolithography of three-dimensional antennas," in *Proc. IEEE Antennas Propag. Soc. Int. Symp.*, vol. 1A. Jul. 2005, pp. 276–279.

[5] N. Delhote, D. Baillargeat, S. Verdeyme, C. Delage, and C. Chaput, "Ceramic layer-by-layer stereolithography for the manufacturing of 3-D millimeter-wave filters," *IEEE Trans. Microw. Theory Tech.*, vol. 55, no. 3, pp. 548–554, Mar. 2007.

[6] N. T. Nguyen, N. Delhote, M. Ettorre, D. Baillargeat, L. Le Coq, and R. Sauleau, "Design and characterization of 60-GHz integrated lens antennas fabricated through ceramic stereolithography," *IEEE Trans. Antennas Propag.*, vol. 58, no. 8, pp. 2757–2762, Aug. 2010.

[7] K. F. Brakora, J. Halloran, and K. Sarabandi, "Design of 3-D monolithic MMW antennas using ceramic stereolithography," *IEEE Trans. Antennas Propag.*, vol. 55, no. 3, pp. 790–797, Mar. 2007.

[8] N. Delhote, D. Baillargeat, S. Verdeyme, C. Delage, C. Chaput, C. Duterte, Y. Abouliatim, and T. Chartier, "Electromagnetic band gap millimeter and sub-millimeter 3D resonators manufactured by ceramic stereolithography," in *Proc. Asia-Pacific Microw. Conf.* Dec. 2007, pp. 1–4.

[9] M. L. Griffith and J. W. Halloran, "Freeform fabrication of ceramics via stereolithography," *J. Amer. Ceram. Soc.*, vol. 79, no. 10, pp. 2601–2608, 1996.

[10] N. Delhote, D. Baillargeat, S. Verdeyme, C. Delage, and C. Chaput, "Innovative shielded high dielectric resonator made of alumina by layer-by-layer stereolithography," *IEEE Microw. Wireless Compon. Lett.*, vol. 17, no. 6, pp. 433–435, Jun. 2007.

[11] N. Delhote, D. Baillargeat, S. Verdeyme, C. Delage, and C. Chaput, "Large experimental bandpass waveguide in 3D EBG woodpile manufactured by layer-by-layer ceramic stereolithography," in *Proc. IEEE/MTT-S Int. Microw. Symp.*, Jun. 2007, pp. 1431–1434.

[12] N. Delhote, D. Baillargeat, S. Verdeyme, C. Delage, and C. Chaput, "Narrow Ka bandpass filters made of high permittivity ceramic by layer-by-layer polymer stereolithography," in *Proc. 36th Eur. Microw. Conf.*, Sep. 2006, pp. 510–513.

[13] R. Rumpf and J. Pazos, "Synthesis of spatially variant lattices," *Opt. Exp.*, vol. 20, no. 14, pp. 15263–15274, 2012.

[14] R. Rumpf, *et al.*, "3D printed lattices with spatially variant self-collimation," *Progr. Electromagn. Res.*, vol. 139, pp. 1–14, 2013.

[15] (2012, Jan. 14), *MakerBot Blog* [Online]. Available: http://www.makerbot.com/blog/tag/key-fob/

[16] *Processing Guide for Printing RFID Antennae* [Online]. Available: http://www2.dupont.com/MCM/en_US/assets/downloads/prodinfo/RFID_ProcessingGuide.pdf

[17] A. Dziedzic and P. Slobodzian. (2011, Apr.). "Modern microelectronic technologies in fabrication of RFID tags," *Radioeng. Proc. Czech Slovak Tech. Univ.* [Online]. 20(1). Available: http://www.radioeng.cz/fulltexts/2011/11_01_187_193.pdf

[18] J. Mirales, D. Espalin, D. Roberson, B. Zinniel, F. Medina, and R. Wicker, "Fused deposition modeling of metals," in *Proc. Solid Freeform Fabricat. Symp.*, Austin, TX, USA, Jan. 2013, pp. 836–845.

[19] M. P. Tonde, "Retrofitting a stereolithography system within a laminar flow hood," M.S. thesis, Dept. Mech. Eng., Univ. Texas, El Paso, TX, USA, 2009.

[20] J. Baker-Jarvis, M. Janezic, and D. C. DeGroot, "High-frequency dielectric measurements," *IEEE Instrum. Meas. Mag.*, vol. 13, no. 2, pp. 24–31, Apr. 2010.

[21] Agilent Technologies. (2009). *Agilent Technologies Impedance Measurement Handbook*, 4th ed., Santa Clara, CA, USA [Online]. Available: http://cp.literature.agilent.com/litweb/pdf/5950-3000.pdf

[22] Agilent Technologies. (2013). *Agilent E4980A Precision LCR Meter 20 Hz to 2 MHz Data Sheet*, Santa Clara, CA, USA [Online]. Available: http://cp.literature.agilent.com/litweb/pdf/5989-4435EN.pdf

[23] Agilent Technologies. (2008). *Agilent 16451B Dielectric Test Fixture Operation Manual*, Santa Clara, CA, USA [Online]. Available: http://cp.literature.agilent.com/litweb/pdf/16451-90020.pdf

[24] *Standard Test Methods for AC Loss Characteristics and Permittivity (Dielectric Constant) of Solid Electrical Insulation*, ASTM Standard D150-11, 2003.

[25] Agilent Technologies. (2011). *Agilent E4991A RF Impedance/Material Analyzer Data Sheet*, Santa Clara, CA, USA [Online]. Available: http://cp.literature.agilent.com/litweb/pdf/5980-1233E.pdf

[26] Agilent Technologies. (2000). *Agilent 16453A Dielectric Material Test Fixture Specification and Service Manual*, Santa Clara, CA, USA [Online]. Available: http://cp.literature.agilent.com/litweb/pdf/16453-90010.pdf

[27] Agilent Technologies. (2001). *Advanced Impedance Measurement Capability of the RF I-V Method Compared to the Network Analysis Method*, Santa Clara, CA, USA [Online]. Available: http://cp.literature.agilent.com/litweb/pdf/5988-0728EN.pdf

[28] W. B. Weir, "Automatic measurement of complex dielectric constant and permeability at microwave frequencies," *Proc. IEEE*, vol. 62, no. 1, pp. 33–36, Jan. 1974.

[29] A. M. Nicolson and G. F. Ross, "Measurement of the intrinsic properties of materials by time-domain techniques," *IEEE Trans. Instrum. Meas.*, vol. 19, no. 4, pp. 377–382, Nov. 1970.

[30] A. Vicente, G. Dip, and C. Junqueira, "The step by step development of NRW method," in *Proc. SBMO/IEEE MTT-S IMOC*, Oct. 2011, pp. 738–742.

[31] T. L. Blakney and W. B. Weir, "Comments on 'Automatic measurement of complex dielectric constant and permeability at microwave frequencies'," *Proc. IEEE*, vol. 63, no. 1, pp. 203–205, Jan. 1975.

[32] J. Baker-Jarvis, "Transmission/reflection and short-circuit line permittivity measurements," Electromagnetic Fields Division, Electronics and Electrical Engineering Laboratory, NIST, Boulder, CO, USA, Tech. Rep. 1341, 2001.

Paul I. Deffenbaugh (M'08) received the B.S. degree in electrical engineering from the Florida Institute of Technology, Melbourne, FL, USA, in 2010, and the M.S. degree in electrical engineering from the University of Texas at El Paso (UTEP), El Paso, TX, USA, in 2011.

He was with Rockwell Collins, Melbourne, FL, USA, as an Intern in reliability and new product development in 2008 and 2009. In 2010, he was with nScrypt, Inc., Orlando, FL, USA, where he met Dr. K. Church, CEO and current Ph.D. Adviser. From 2010 to 2011, he studied 3-D printing and direct-print technologies at nScrypt while attending master's classes at UTEP before eventually moving to El Paso to research full time in the W. M. Keck Center for 3-D Innovation. His current research interests include 3-D printing and its applications in microwave electromagnetics.

Raymond C. Rumpf (M'93) received the B.S. and M.S. degrees in electrical engineering from the Florida Institute of Technology, Melbourne, FL, USA, in 1995 and 1997, respectively, and the Ph.D. degree in optics from the University of Central Florida, Orlando, FL, USA, in 2006.

He joined University of Texas at El Paso, El Paso, TX, USA, in 2010, to form the EM Lab within the W. M. Keck Center for 3-D Innovation. His research is focused on developing revolutionary electromagnetic devices and technologies enabled by additive manufacturing (3-D printing). His work entails device theory, modeling and simulation, manufacturing, materials, and simulation. His current research interests include metamaterials, awkward and multifunctional antennas, 3-D circuits, and all-dielectric electromagnetics.

Kenneth H. Church (M'88) received the B.S. degree in physics and electrical engineering from Oklahoma Christian University, Oklahoma City, OK, USA, in 1988 and 1989, respectively, and the master's and Ph.D. degrees from Oklahoma State University, Stillwater, OK, USA, in 1991 and 1994, respectively.

He joined University of Texas at El Paso, El Paso, TX, USA, in 2009, to expand the capabilities within the W. M. Keck Center for 3-D Innovation. His research is focused on functional 3-D RF devices, direct printing, 3-D printing and RF materials. He has worked in metamaterials, antenna optimization, electronic packaging, and sensors. His current research interests include miniaturized and 3-D spatially variant RF electronics.